

Vortex dynamics in jets from inclined nozzles

D. R. Webster and E. K. Longmire

Department of Aerospace Engineering and Mechanics, University of Minnesota, Minneapolis, Minnesota 55455

(Received 13 August 1996; accepted 14 November 1996)

Experimental tests were performed on round jets exiting inclined nozzles at a Reynolds number of 9000. Both natural jets and jets forced with single frequencies corresponding to $St_D = 0.25, 0.5, 0.75,$ and 1.0 were examined. In the natural case, the nozzle incline caused a mild increase in the radial spreading in the plane of azimuthal symmetry. The forcing amplified the asymmetric radial spreading by altering the vortex structure. In general, the inclined vortex rings rolled up at an angle slightly smaller than the nozzle incline angle. As the rings moved downstream, they migrated away from the jet centerline and their incline angle increased. Vortex rings generated at $St_D = 0.5$ did not pair because that Strouhal number was near the ‘‘preferred’’ mode. For nozzles with slight inclines, forcing at larger Strouhal numbers led to pairing near $x/D = 2$ in order to achieve the ‘‘preferred’’ mode. For nozzles with larger inclines, the vortex cores broke down before pairing could occur. Forcing at a lower Strouhal number ($St_D = 0.25$) yielded ring formation at $St_D = 0.5$ and subsequent pairing. Increasing the incline angle moved the pairing location closer to the nozzle lip. Also, the pairing process was found to depend on the nozzle incline angle. © 1997 American Institute of Physics. [S1070-6631(97)01903-X]

I. INTRODUCTION

A jet of fluid exiting a round nozzle is unstable to the surrounding fluid and reacts by forming either axisymmetric or helical structures. The formation frequency of the structures normally is determined by the initial shear layer thickness.^{1,2} The form of the initial and subsequent structures, however, can be influenced by either forcing schemes or nozzle geometry.

Many researchers, including Crow and Champagne,³ Browand and Laufer,⁴ Bouchard and Reynolds,⁵ Hussain and Zaman,⁶ Arbey and Ffowcs Williams,⁷ and Mankbadi,⁸ have investigated the effects of axial forcing on round jets. This type of forcing normally encourages the formation of axisymmetric vortex rings. The amplitude and frequency of the forcing pattern determine the vortex ring strength, spacing, and pairing locations. Orbital forcing has been employed to perturb the axisymmetry of round jets. Corke and Kusek⁹ used orbital forcing to induce helical structures, while Lee and Reynolds¹⁰ and Parekh, Leonard, and Reynolds¹¹ combined axial and orbital forcing to produce blooming and bifurcating jets. In this case, the forcing generated vortex rings with slight asymmetries in position and shape, and neighboring rings induced one another to move on angled paths with respect to the jet centerline.

Nozzle geometry has also been used to control the vortex dynamics in jets. In some cases, the control objective has been to accelerate the breakdown of large structures into smaller scales. For example, tabs that project into the flow near the nozzle lip generate longitudinal structures that enhance mixing and accelerate the breakdown of axisymmetric vortex rings.^{12,13} Wavy or fluted nozzle shapes¹⁴ and the corner regions of square nozzles¹⁵ produce similar effects. Jets from elliptic nozzles have also been studied and were found to significantly increase the mass entrainment due to the non-axisymmetric vortex ring formation.^{16,17}

Wlezien and Kibens¹⁸ introduced the phrase ‘‘indetermi-

nate origins’’ to describe nozzles in which the axial position of the trailing edge varies with azimuth. In previous work, this type of nozzle shape has been used not only to initiate longitudinal secondary structures, but also to ‘‘bend’’ primary vortex rings. Studies on stepped and sawtooth nozzles (Wlezien and Kibens,¹⁸ Kibens and Wlezien,¹⁹ and Longmire and Duong²⁰) revealed that trailing edges with sharp discontinuities in axial position could be used to generate bent vortex rings and irregular helical structures. In most cases, the nozzle lip discontinuity appeared to promote longitudinal vorticity, which intermittently entrained fluid from the ambient into the jet core. When the flow was forced axially at a subharmonic of the most unstable roll-up frequency, neighboring vortex rings induced one another into opposing orientations leading to a bifurcation of the jet. Thus, the axial momentum could be redistributed into distinct primary and secondary columns with opposing radial directions. The crown-shaped nozzles of Longmire *et al.*,²¹ which had sharp discontinuities in the slope of the lip, produced longitudinal structures somewhat similar to those observed downstream of nozzles with tabs. In this case, however, the longitudinal structures were always coupled with primary vortices that were either planar or azimuthally wavy depending on tooth length and forcing frequency.

In the current work we address the simplest indeterminate origin geometry: inclined nozzles with continuous lip location and slope. Hence, the longitudinal structures associated with nozzle discontinuities are unlikely to occur. In previous work, Wlezien and Kibens¹⁸ and Kibens and Wlezien¹⁹ found a nonaxisymmetric increase in jet spreading that was amplified by acoustical excitations. Their flow visualization photographs revealed two basic instability types in the near field of jets from inclined nozzles. In the case of relatively long instability wavelengths compared to the incline length ($\lambda/L > 0.5$, approximately), the shear layer rolled up parallel to the nozzle lip thus leading to continuous inclined vortex

rings. Although some variation was observed, the inclined rings tended to evolve downstream into an axisymmetric orientation. Wlezien²² found that portions of a given ring paired with either the leading or trailing neighbor depending on the azimuthal position. This asymmetric pairing process reorganized the jet column vorticity into nearly axisymmetric structures for $x/D > 4$. The second instability type was observed when the instability wavelength was small compared to the incline length ($\lambda/L < 0.5$). Once the shear layer at the azimuthal location where the nozzle was shortest became unstable, it triggered locally coherent instabilities at other azimuthal locations. The structure formed normal to the jet axis, and the phase relation was referenced to the initial instability. The extent to which the structure was coherent around the circumference was a function of the shear layer thickness. Acoustical excitation at certain frequencies produced combinations of the two basic instability types in which high-frequency waves normal to the jet axis were observed in what appeared to be the braid region of a lower-frequency inclined structure.

The inclined nozzle jet flow is analogous to planar mixing layers with skewed trailing edges, which have been examined by Kibens *et al.*²³ and Gründel.²⁴ In this work, the instability mechanisms and subsequent vortex structure appeared similar to that in the jet studies. In an acoustically excited mixing layer with a trailing edge at 45° to the mean flow direction, Kibens *et al.*²³ again observed two types of vortex formation. At lower forcing frequencies, vortices formed parallel to the trailing edge, while at higher forcing frequencies, vortices formed perpendicular to the mean flow. When the flow was not forced, both types of vortices occurred.

In this study we address new questions about the structure of jets from inclined nozzles. Specific objectives are to determine the effects of incline angle, forcing frequency, and forcing amplitude on the near-field vortex ring formation and propagation. Of particular interest is the influence of flow parameters on vortex ring orientation, interaction, and pairing. We are also interested in the effect of the vortex structure on radial spreading and entrainment.

II. FACILITY AND EXPERIMENTAL TECHNIQUES

The experiments were conducted in the recirculating water jet facility shown in Fig. 1. The jet flowed into a Plexiglas tank with 965 mm length, 760 mm width, and 710 mm height. The influence of the tank walls and free surface on the free jet was negligible. Water was removed from the tank by four suction pipes (50.8 mm i.d.), each containing 22 holes (8 mm diam) arranged in two columns 120° apart. This arrangement ensured that equal amounts of flow passed through each pipe. The suction pipes were connected to a collector chamber (102 mm i.d. circular cross section) with flexible tubing. The flow was driven with a magnetic-drive 1/10 hp pump. The pump was mechanically isolated from the tank and pump vibration effects were minimal. Downstream of the pump, the flow rate was controlled with a 25.4 mm PVC gate valve and measured with a rotameter (0–10 gpm).

The jet plenum had a 102 mm i.d. circular cross section that contained two honeycomb arrays. The flow passed

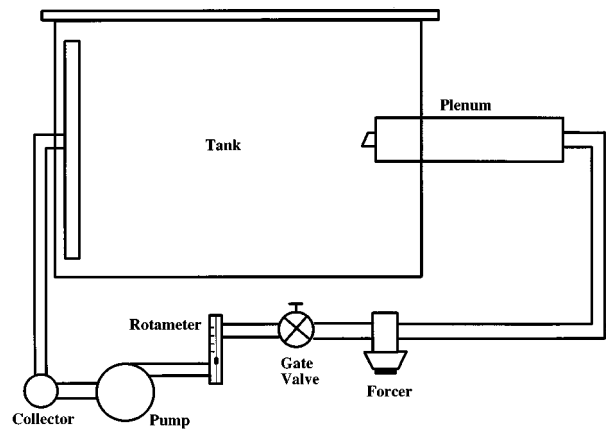


FIG. 1. Recirculating water jet facility.

through an axisymmetric contraction (11.5 to 1 area reduction) with an overall length of 152 mm and a wall profile fit to a fifth-order polynomial. The inner diameter of the contraction exit was 30 mm, which matched the jet nozzles exactly. The jet nozzle geometry is shown in Fig. 2. The PVC nozzles had an inner diameter of 30 mm and a wall thickness of 1.7 mm. For each nozzle, the development length was approximately 26 mm to the shortest nozzle lip location. The unforced turbulence intensity at the centerline of the jet exit was 0.6% of the nominal velocity.

The forcer consisted of a 76 mm diam piston driven by an 80 W subwoofer speaker. The speaker/piston apparatus was controlled by a constant frequency signal generated by a computer and amplified externally. The amplitude of the velocity oscillation superimposed on the flow by the forcer was measured by placing a hot-film probe at the jet nozzle exit. The probe was connected to a TSI constant temperature an-

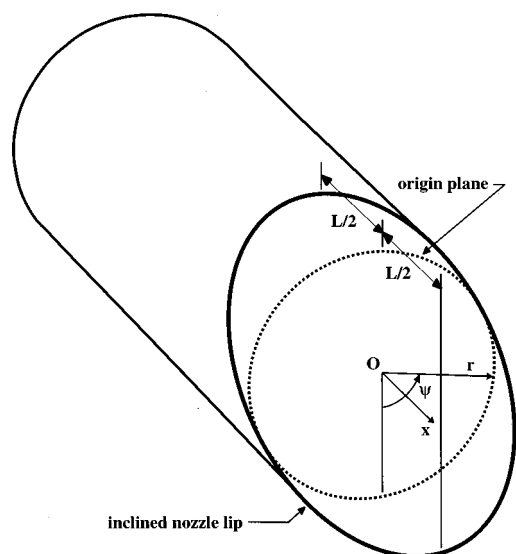


FIG. 2. Perspective view of the inclined jet nozzle. Here O denotes the coordinate origin at the nozzle centerline and incline midpoint; L is the incline length.

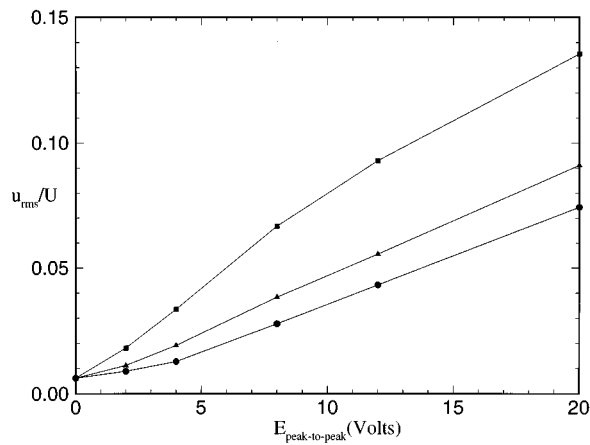


FIG. 3. Flow response at the jet exit to forcing; ■ 2.5 Hz ($St_D = 0.25$); ▲ 5 Hz (0.5); ● 10 Hz (1.0). E is the voltage input to the speaker.

emometer (model IFA-100) operating at a resistance ratio of 1.08. Figure 3 shows that the flow response amplitude was dependent on the forcing frequency.

Flow visualization was performed by injecting a pH basic bromothymol blue dye solution (15 g of NaOH and 0.4 g of bromothymol blue per liter of solution) through ports at the inflection point of the contraction. The blue dye solution mixed with dilute hydrochloric acid in the water tank resulting in a yellowish background color. Molecular diffusion was small compared to turbulent mixing, thus the dye streaks tracked the shear flow until transition to turbulence. The evolving dye streaks were captured on S-VHS format tape with a Panasonic video camera.

Instantaneous velocity fields were measured using particle image velocimetry (PIV). Illumination sheets were generated with two pulsed Nd:YAG lasers arranged side by side. The beam paths were combined with a polarization beam-splitter, such that the on-axis beam was transmitted by the ‘‘splitter’’ while the off-axis beam was reflected. Each laser pulsed at 10 Hz with a pulse duration of 7 ns. The delay between pulses was 1.0 ms. The energy output per pulse was approximately 100 mJ. A 1 m focal length spherical lens and a 50 mm focal length cylindrical lens were used to create each illumination sheet. The thickness of each sheet was approximately 1 mm throughout the photographed flow field. The water was seeded with TiO_2 particles with a specific gravity of 3.5 and nominal diameter of 3 μm . The inertial time constant of the particles was approximately 2 μs , and the settling velocity was 12 $\mu\text{m/s}$, both of which were negligibly small for this flow.

Single images of double-pulse events were acquired with a Kodak DCS 420M digital camera and Nikon AF Micro-Nikkor lens with 60 mm focal length. The monochrome pixel array size was 1012×1524 , and the pixel depth was ten bits. The ISO equivalent was 800, and the aperture setting was $f5.6$. The camera and a rotating mirror were located in a plane parallel to the illumination sheet. The focal distance was 659 mm. The resulting resolution for the digital images was 9.45 pixels per millimeter in the illumination plane. The rotating mirror (45×54 mm) imposed an artificial shift on

the image in order to resolve directional ambiguity and to alleviate the large-velocity disparity between the jet core and ambient fluid. The mirror position was controlled with a Cambridge Technology coil galvanometer-based scanner (Model 6650). The rotation rate of the mirror was 0.87 rad/s. Hence, the artificial shift corresponded to 11 pixels on the array (or a velocity of 1150 mm/s).

Timing and control signals were generated with a Macintosh Iix computer and a National Instruments NB-MIO-16X (12-bit DAC) board. Separate DAC channels were used to generate a sine wave for the forcer and a sawtooth wave for the rotating mirror controller. The relative phase of the sine wave signal was controlled in order to measure specific phases of the forced cycle. An external timing circuit was triggered on the down-edge of the sawtooth signal. The timing circuit controlled the laser pulsing and camera shutter such that the camera recorded the images when the mirror was nominally at 45° .

Acquired images were stored on a PCMCIA Type III card inside the camera and subsequently downloaded with Adobe Photoshop to a Macintosh Iicx computer through the SCSI interface. On a Silicon Graphics Indy workstation, software from Flow Diagnostics Inc. was used to calculate the average pixel displacement of image pairs in each interrogation area via a spatial autocorrelation method. Interrogation areas were 64×64 pixels, corresponding to a spatial resolution of 6.8×6.8 mm. The overlap of the interrogation area was 50%, so that a 31×47 vector field was calculated for each image file. No interpolated vectors were substituted into the field. The time delay between laser pulses and the image magnification were then used to calculate the velocity at each point. Fifteen instantaneous files were ensemble averaged for each case. The uncertainty of the ensemble-averaged velocity measurements was estimated to be $\pm 3\%$ of the nominal jet velocity. The largest contribution to this estimate was the uncertainty in the particle displacement measurement. The uncertainty of the subsequent measurements of vortex ring incline angle and position are estimated to be $\pm 1^\circ$ and $\pm 0.01D$, respectively.

III. RESULTS

The cylindrical coordinate system (r, ψ, x) is shown in Fig. 2. The origin was along the jet centerline at the average axial lip location denoted with the dotted line. The ψ coordinate was zero at the location where the nozzle lip was longest, and thus, $\psi = \pi$ where it was shortest. The reference nozzle (0° incline angle) and nozzles with incline lengths (L in Fig. 2) of $D/4$ (14°), $D/2$ (26°), $3D/4$ (37°), and D (45°) were tested extensively. Additional tests were performed on longer incline lengths up to $2D$ (63°). The PIV measurements were performed in two planes: $\psi = 0, \pi$ and $\psi = \pi/2, 3\pi/2$. The nominal jet centerline exit velocity (U) was 304 mm/s corresponding to $Re_D = 9000$.

A. Unforced flow

The momentum thickness of the initial shear layer was estimated from the velocity profile at the reference nozzle exit to be 0.32 mm. Following the linear stability analysis of Michalke,¹ the most unstable frequency was 16 Hz

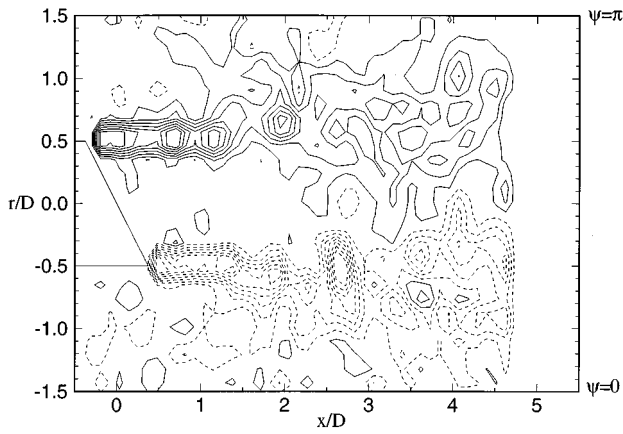


FIG. 4. Instantaneous vorticity field for the unforced 3D/4 nozzle. The figure shows 14 contour levels ranging from $-4U/D$ to $4U/D$.

($St_\theta=0.017$). The wavelength measured from the flow visualization yielded an instability frequency within $\pm 3\%$ of this value, indicating that the unforced reference jet behavior agreed well with inviscid theory.

Figure 4 shows an instantaneous vorticity field for the unforced jet from the 3D/4 nozzle, which is indicative of the behavior from the other nozzles. Three inclined vortex rings are evident: two centered around $x/D = 1.25$ and one at $x/D = 2.5$. The incline angle of the rings nearly matches that of the nozzle, indicating that the instability waves at each azimuthal location were dictated by the local distance from the nozzle and hence form parallel to the nozzle lip.

Figure 5(a) shows an ensemble-averaged velocity field

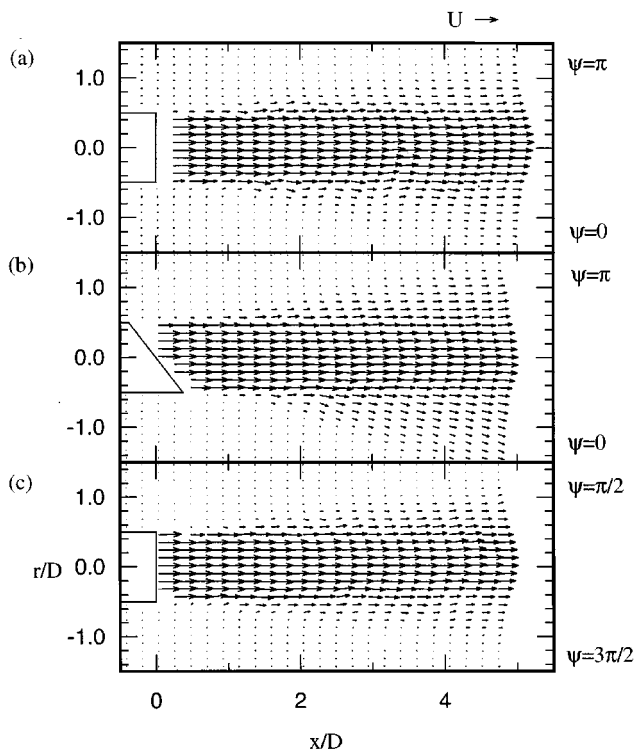


FIG. 5. Ensemble-averaged velocity field for the (a) unforced reference nozzle, and (b) and (c) orthogonal planes for the unforced 3D/4 nozzle.

for the unforced reference nozzle. For clarity, only every second vector is plotted in the x direction in all vector plots. Individual vortex ring structures were averaged during the ensembling process and do not appear in the figure. The jet is symmetric as expected, although the shear layer appears slightly wavy owing to the relatively small number of ensembled fields. [The number (15) of instantaneous velocity fields used to ensemble average was sufficient to achieve the stated measurement uncertainty.] Figure 5(b) shows increased radial spreading from the 3D/4 nozzle relative to the reference nozzle especially in the $\psi=0$ half-plane. In contrast, Fig. 5(c) indicates that the $\psi=\pi/2$ and $3\pi/2$ half-planes behave symmetrically. The flow field in this plane strongly resembles the unforced reference flow, and the spread rate is similar. The overall effect of the nozzle is an elongation of the jet column cross section into an oval shape. This asymmetric elongation of the jet column agrees with the observations of Wlezien and Kibens.¹⁸

B. Forced flow

Flow visualization was performed for each nozzle incline for the frequency and amplitude combinations shown in Fig. 3. The flow characteristics remained qualitatively similar among the forcing amplitudes explored. As discussed below, the vortex structure consisted of continuous inclined rings. Increasing the forcing amplitude increased the vorticity in the core of the ring; however, the vortex dynamics remained essentially unchanged.

The PIV measurements were conducted for each nozzle by supplying the forcer with an 8 V peak-to-peak signal. A limited number of cases with a 20 V signal were examined in order to verify that qualitatively similar behavior was observed. For the 8 V case, the velocity perturbation at the nozzle exit was $u_{rms}/U = 0.06$ for 2.5 Hz ($St_D = 0.25$), 0.04 for 5 Hz ($St_D = 0.50$), and 0.03 for 10 Hz ($St_D = 1.0$). In all cases, the vortex structure locked into a repeatable pattern that could be sampled at specified phases in the forcing cycle. The phase notation, Φ , which is shown for each figure, was specified relative to the sine wave signal supplied to the forcer.

1. $St_D=0.5$

The case with Strouhal number equal to 0.5 (5 Hz) is discussed first because the vortex dynamics are the least complicated. Figure 6 shows velocity fields for the D nozzle in the two orthogonal planes. Velocity perturbations resulting from the vortex ring structure appear in the shear layer of each half-plane spaced at approximately D . The perturbations in the $\psi=\pi/2$ and $3\pi/2$ half-planes have reflective symmetry, while the nozzle geometry prevents symmetry between the $\psi=0$ and π half-planes. By comparing orthogonal views, the continuous inclined vortex ring structure can be reconstructed. The inclined vortex rings are consistent with those observed by Kibens and Wlezien¹⁹ for long instability wavelengths compared to the incline length.

At this Strouhal number, the vortex ring dynamics are similar for each nozzle incline. Continuous rings form nearly parallel to the inclined nozzle lip, and the rings do not pair. (In the current experiment, the Reynolds number and shear

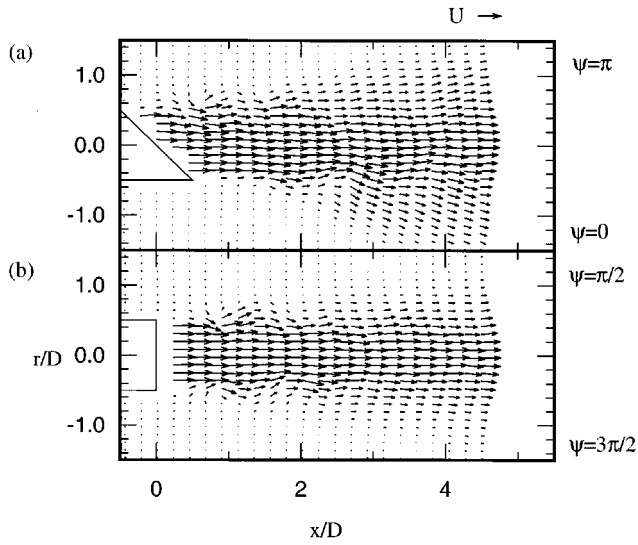


FIG. 6. Ensemble-averaged velocity field for the D nozzle forced at $St_D = 0.50$ (5 Hz), $u_{rms}/U = 0.04$. (a) and (b) are orthogonal planes at phase $\Phi = 3\pi/2$.

layer thickness agree closely with those of Browand and Laufer,⁴ who observed a “preferred” mode of $St_D = 0.5$ in a simple round jet.) Shown in Figs. 7 and 8 are the vorticity fields for the $D/4$ and D nozzles. The vortex cores, which are clearly identifiable, are spaced at approximately one diameter. Two basic characteristics of the vortex ring evolution are clear. The incline angle of each ring increases as it moves downstream, and each vortex ring migrates toward the $\psi = \pi$ half-plane. Figure 9 reveals these trends explicitly by plotting the incline angle and radial position as a function of downstream position for each nozzle.

In Fig. 9(a), the vortex incline angle has been normalized by the nozzle incline angle so that the relative change

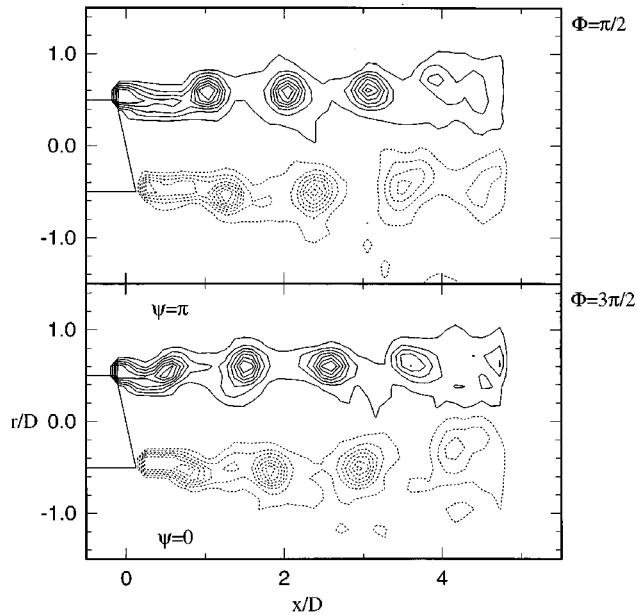


FIG. 7. Ensemble-averaged vorticity field for the $D/4$ nozzle forced at $St_D = 0.50$ (5 Hz), $u_{rms}/U = 0.04$ for two phases. The figure shows 14 contour levels ranging from $-5.5U/D$ to $5.5U/D$.

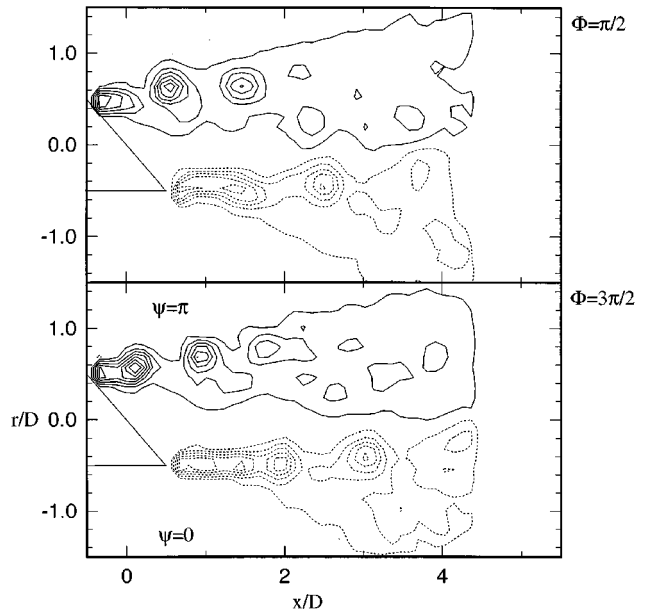


FIG. 8. Ensemble-averaged vorticity field for the D nozzle forced at $St_D = 0.50$ (5 Hz), $u_{rms}/U = 0.04$ for two phases. The figure shows 14 contour levels ranging from $-5.5U/D$ to $5.5U/D$.

can be compared among nozzles. For each case, the incline angle of the vortex ring is slightly less than the nozzle incline angle for $x/D < 1.5$. The fact that the ring deviates slightly from parallel alignment indicates that the farthest upstream roll-up (at $\psi = \pi$, where the nozzle is shortest) mildly encourages the roll-up at other circumferential locations. Once formed, the incline angle of each ring increases monotonically for all nozzles, and the effect is stronger for the less inclined nozzles. Vortex rings from the $D/4$ nozzle achieve

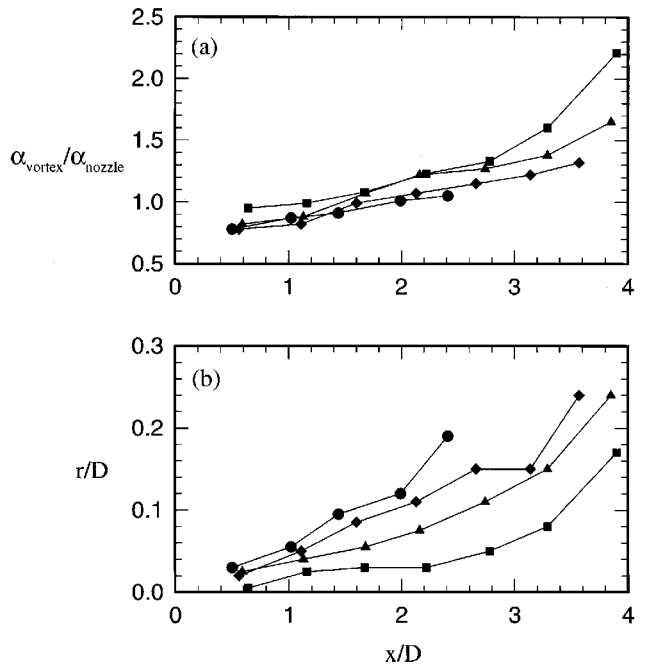


FIG. 9. (a) Relative incline angle, and (b) radial position of the vortex ring as a function of downstream position. Forcing at $St_D = 0.50$ (5 Hz) for the ■ $D/4$, ▲ $D/2$, ◆ $3D/4$, and ● D nozzles.

more than twice the nozzle incline angle, while rings for the D nozzle reach a maximum of 5% greater than the nozzle incline before the cores break down. The flow visualization of Kibens and Wlezien¹⁹ revealed the opposite effect, namely that the inclined vortex rings tended to evolve into an orientation normal to the jet. Wlezien²² found that the evolution to an axisymmetric structure was a result of a vortex ring pairing with its upstream neighbor in the $\psi=0$ half-plane and its downstream neighbor in the $\psi=\pi$ half plane around $x/D = 2$. In contrast, no pairing was observed for the current jet flow when forced at $St_D = 0.5$. For the Strouhal number discussed below, pairing was observed, but never in the manner observed by Wlezien.²²

Figure 9(b) shows that, for all of the nozzles examined, the midpoints of the vortex ring migrate toward the $\psi=\pi$ half-plane. This is quite different from the reference nozzle case in which axisymmetric rings remain essentially centered on the jet axis. The inclined orientation of the rings results in a self-induced trajectory into the $\psi=\pi$ half-plane. The rate of migration into the $\psi=\pi$ half-plane is greater for the more inclined nozzles because the self-induced trajectory is more severely off the jet centerline for a more inclined vortex ring.

By comparing Figs. 7 and 8, it is clear that the cores of the initially more inclined rings break down much closer to the nozzle. One intriguing hypothesis is that the incline angle of the rings may increase to an universal maximum preceding breakdown. This did not appear to be the case, however, since the maximum incline angle of the rings varied significantly with Strouhal number and nozzle incline angle. (The maximum incline angle observed for the $St_D = 0.5$ case was 49° .) A more agreeable idea comes from the recent experiments of Liepmann and Gharib²⁵ and the inviscid vortex filament simulation of Martin and Meiburg.²⁶ They have shown that, for a simple round jet, longitudinal vorticity perturbations grow in the highly strained braid regions between the ring cores and that the longitudinal vorticity is fundamentally important to the breakdown of the cores. By inclining the vortex rings, additional strain rates are introduced to the braid regions. In particular, the terms containing azimuthal derivatives are nonzero for inclined rings. Although the strain rate tensor was not measured, the accelerated core breakdown for more inclined nozzles indicates that the additional strain rates were increasing the growth rate of longitudinal vorticity perturbations in the braid region.

2. $St_D = 0.75$ and 1.0

Flow visualization was performed for each nozzle with forcing at $St_D = 0.75$ (7.5 Hz) and $St_D = 1.0$ (10 Hz). The vortex structure again formed as continuous rings inclined nearly parallel to the nozzle lip. The vortex ring spacing was $D/2$ and $3D/4$ for $St_D = 1.0$ and 0.75, respectively. In both cases, the rings paired around $x/D = 2$ in order to achieve a “preferred” mode. Only results for the $St_D = 1.0$ case will be discussed here since the $St_D = 0.75$ case behaved similarly, except for the absolute ring spacing.

Figure 10 shows an instantaneous vorticity field forced at $St_D = 1.0$ from the $D/4$ nozzle. Ensemble averaging was inappropriate for this case because neighboring vortex rings pair to a $St_D = 0.5$ spacing, hence two possible flow fields

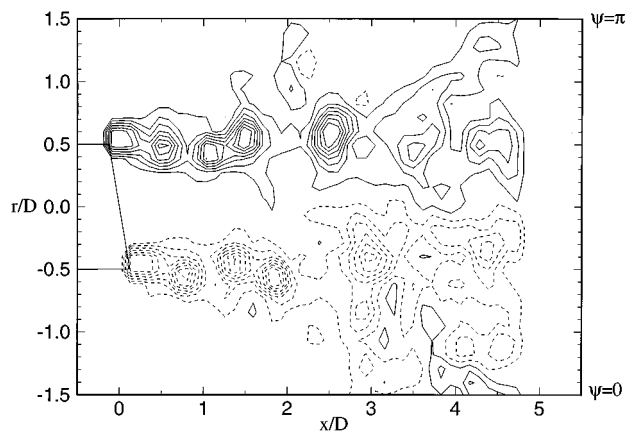


FIG. 10. Instantaneous vorticity field for the $D/4$ nozzle forced at $St_D = 1.0$ (10 Hz), $u_{rms}/U = 0.03$ at phase $\Phi = \pi/2$. The figure shows 14 contour levels ranging from $-5U/D$ to $5U/D$.

could be observed at a given phase in the 10 Hz cycle. In addition, the nonlinear roll-up process led to some variation of the vortex ring pairing location. For the example shown, the initial spacing of the inclined vortex rings is $D/2$. Two rings are beginning to pair around $x/D = 1.5$. An inclined ring is observed downstream at $x/D = 2.8$ as a result of a previous pairing process. Distinct coherent vortex cores were not observed downstream of this point in this or any other instantaneous field. Thus the coherent structure breaks down earlier than for $St_D = 0.5$, in which case vortex cores were clearly identifiable beyond $x/D = 4$. The reference case behaves essentially in the same manner; the initial vortex rings spaced at $D/2$ pair between $x/D = 1.5$ and 2. Then, the coherent paired ring cores break down between $x/D = 3$ and 4.

As the nozzle incline angle increases, the pairing process is suppressed. Figure 11 shows an instantaneous vorticity field for the D nozzle forced at $St_D = 1.0$. Again the initial spacing of the inclined vortex rings is $D/2$. No distinct pairing was observed in any instantaneous fields. The coherent vortex structure breaks down within two diameters of the

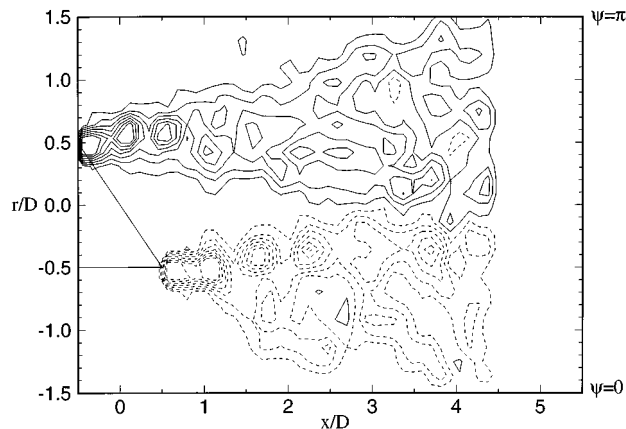


FIG. 11. Instantaneous vorticity field for the D nozzle forced at $St_D = 1.0$ (10 Hz), $u_{rms}/U = 0.03$ at phase $\Phi = \pi/2$. The figure shows 14 contour levels ranging from $-4U/D$ to $4U/D$.

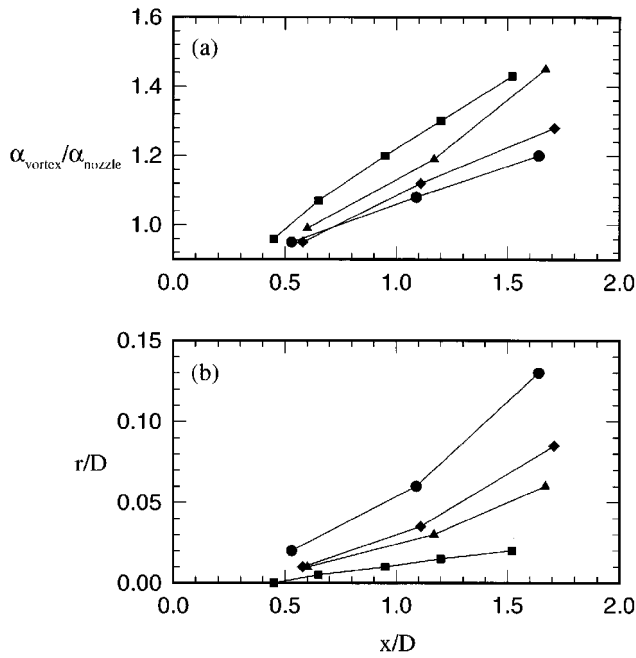


FIG. 12. (a) Relative incline angle, and (b) radial position of the vortex ring as a function of downstream position. Forcing at $St_D = 1.0$ (10 Hz) for the \blacksquare $D/4$, \blacktriangle $D/2$, \blacklozenge $3D/4$, and \bullet D nozzles.

nozzle lip due to the additional strain rates in the braid region resulting from the inclined orientation. Hence, the opportunity to pair and achieve the ‘‘preferred’’ mode simply does not exist. The amplitude of the forcing signal was increased to 20 V, corresponding to $u_{rms}/U = 0.07$, in order to evaluate the effect of amplitude on this case. Essentially the same behavior was observed.

In agreement with the $St_D = 0.5$ case, the vortex incline angle increases with downstream distance and each vortex ring migrates into the $\psi = \pi$ half-plane. Figure 12 shows the incline angle and radial position to about $x/D = 1.5$. Beyond this point, the vortex rings either pair or break down depending on the nozzle incline angle. The vortex incline angle starts slightly smaller than the nozzle incline angle and then increases monotonically. The increase is greater for the less inclined nozzles. The migration into the $\psi = \pi$ half-plane is greater for the more inclined nozzles because of the trajectory of the self-induced motion. These observations are consistent with those for the $St_D = 0.5$ case.

Kibens and Wlezien¹⁹ observed ‘‘locally coherent instabilities’’ aligned normal to the jet axis when $\lambda/L < 0.5$. In the current experiments, nominal vortex ring spacing for the $St_D = 1.0$ case was $D/2$. Thus, the wavelength to incline ratio was $\lambda/L = 0.5$ for the D nozzle (Fig. 11). Continuous inclined vortex rings were reconstructed from the orthogonal data planes for these conditions. In an attempt to generate instabilities perpendicular to the jet axis, nozzles with incline lengths up to $2D$ ($\lambda/L = 0.25$ for $St_D = 1.0$) were tested. All cases yielded continuous inclined vortex rings. Furthermore, as the incline angle increased, the trends reported above continued: The inclined vortex rings migrated into the $\psi = \pi$ half-plane, the incline angle increased downstream, and the breakdown of coherent structure was accelerated. The differ-

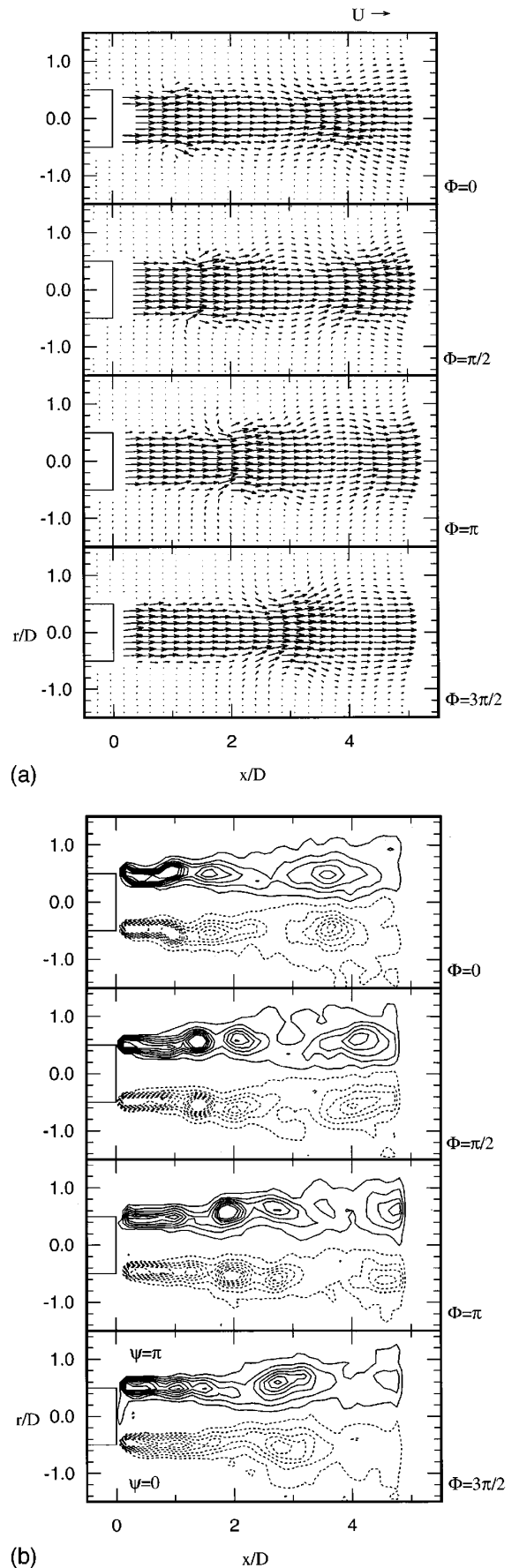


FIG. 13. Ensemble-averaged (a) velocity field, and (b) vorticity field (14 contour levels ranging from $-4U/D$ to $4U/D$) for the reference nozzle forced at $St_D = 0.25$ (2.5 Hz) and $u_{rms}/U = 0.06$. Four phases are shown.

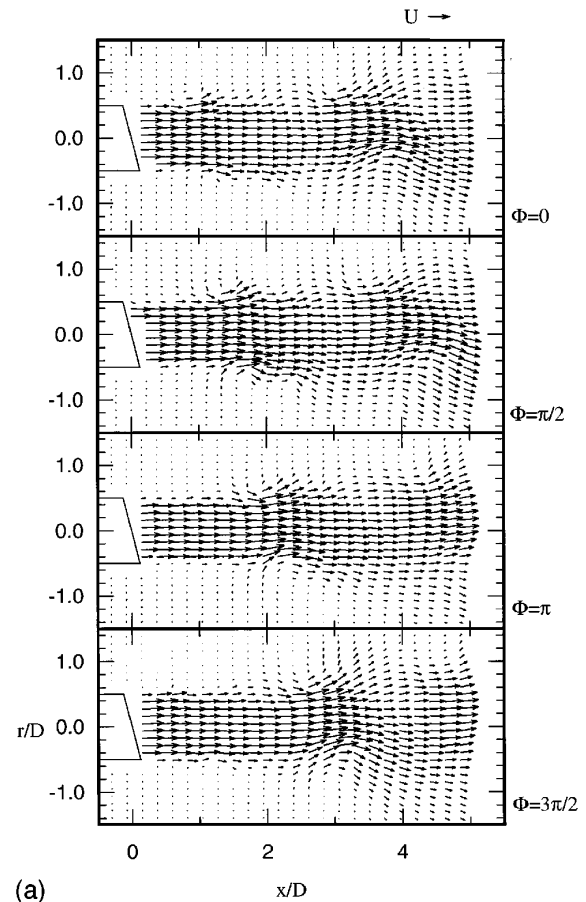
ing results observed in the two studies may be explained by two important differences in the experimental setup. First, Kibens and Wlezien¹⁹ employed three independent forcing procedures, including a nozzle lip excitation technique that was quite different from the current simple axial forcing. Second, Kibens and Wlezien¹⁹ had a much thinner shear layer (relative to the jet diameter) because they operated an air jet at larger Re_D . They varied the shear layer thickness somewhat and found that a thicker shear layer allowed the jet structure to be organized around the entire circumference. The shear layer thickness for the current water jet may have been sufficiently thick that continuous inclined vortex rings were formed for the tested nozzles.

3. $St_D = 0.25$

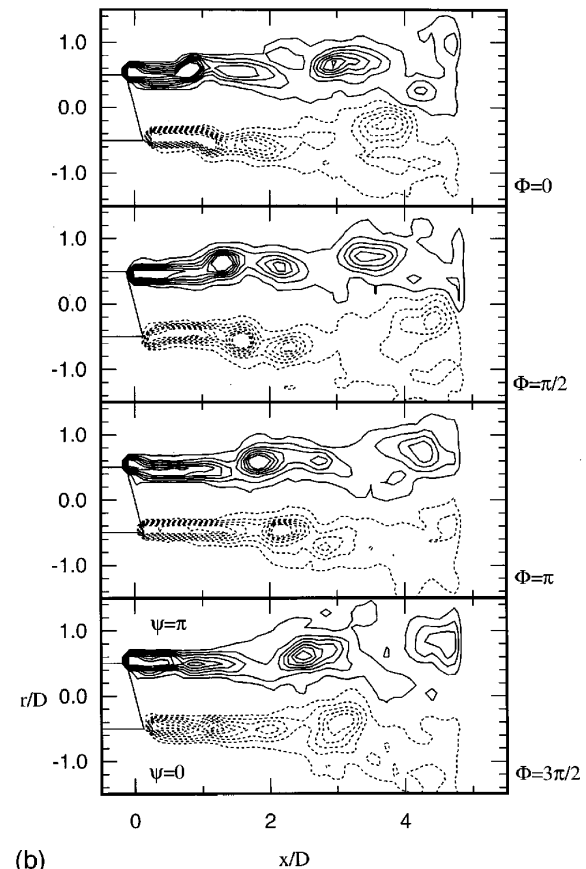
Figure 13 shows four equally spaced phases of the ensemble-averaged velocity and vorticity fields for the reference nozzle forced at $St_D = 0.25$ (2.5 Hz). The vortex ring evolution can be observed in the vorticity plots. Vortex rings initially form at a frequency of 5 Hz, then pair axisymmetrically at approximately $x/D = 2.5$. In agreement with previous authors' observations, the trailing ring reduces its diameter and speeds up until it combines with the lead vortex ring, which has decreased its speed and increased its diameter. The velocity vectors show that the jet column remains essentially symmetric and that the axial momentum has spread mildly in the radial direction by $x/D = 4$. Weak entrainment and ejection are observed on the upstream and downstream side of each ring core, respectively.

For the $D/4$ nozzle shown in Fig. 14, the incline angle of the vortex rings affects both the pairing process and the jet column shape. In the vector plots, the axial velocity just downstream of the ring cores shows a nearly linear variation between the $\psi = \pi$ (small) and 0 (large) half-planes. In addition, the velocity vectors near the combined vortex ring (e.g., at $x/D = 3.5$ in phase $\Phi = 0$) are tilted into the $\psi = \pi$ half-plane. Upstream and downstream of the ring, the vectors are nearly aligned with the jet axis. The net result is a jet column that appears serpentine in the neighborhood of the paired ring. The entrainment on the upstream side of each ring is mild as in the reference nozzle case. However, the radial ejection of fluid on the downstream side of each inclined ring is greatly enhanced, particularly for $x/D > 3$ and the $\psi = 0$ half-plane. This is consistent with the increased radial spreading in the $\psi = 0$ half-plane for the unforced flow discussed above.

The axisymmetry of the vortex pairing is also altered. The pairing sequence shown in Fig. 14(b) occurs as follows: Two vortex rings with spacing D roll up nearly parallel to the inclined nozzle lip. The leading ring migrates into the $\psi = 0$ half-plane while its incline angle decreases. At the same time, the trailing ring migrates into the $\psi = \pi$ half-plane as its incline angle increases. The cores pair around $x/D = 2.5$ in the $\psi = 0$ half-plane. In the $\psi = \pi$ half-plane, the cores are moving apart as a result of the incline angles diverging. Nevertheless, the cores in phase $\Phi = 3\pi/2$ appear to have paired. Although the process is not clear from the PIV data, the flow visualization indicates that the weakened leading core is rapidly ejected radially outward and then spins



(a)



(b)

FIG. 14. Ensemble-averaged (a) velocity field, and (b) vorticity field (14 contour levels ranging from $-4U/D$ to $4U/D$) for the $D/4$ nozzle forced at $St_D = 0.25$ (2.5 Hz) and $u_{rms}/U = 0.06$. Four phases are shown.

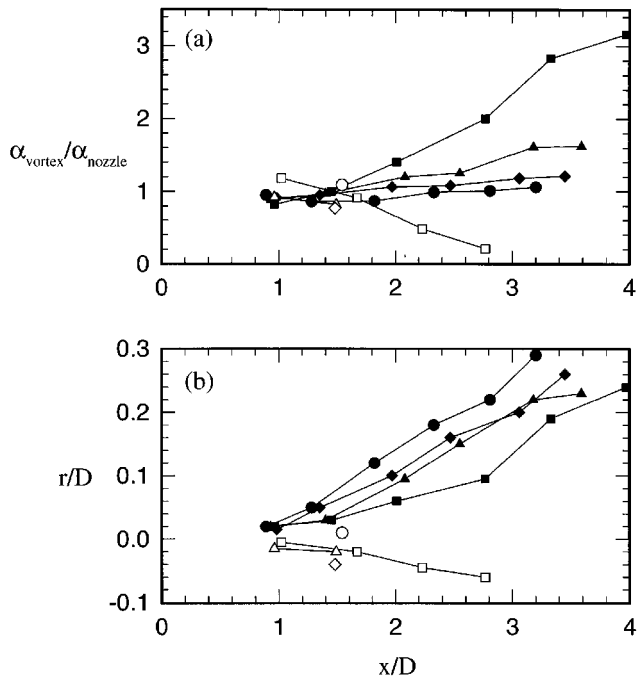


FIG. 15. (a) Relative incline angle, and (b) radial position of the vortex ring as a function of downstream position. Forcing at $St_D = 0.25$ (2.5 Hz) for the \blacksquare $D/4$, \blacktriangle $D/2$, \blacklozenge $3D/4$, and \bullet D nozzles. Solid symbols are for the trailing and paired vortex ring and hollow symbols are for the leading vortex ring.

around the trailing core. As the combined vortex ring moves downstream, the incline angle increases, and the ring migrates into the $\psi = \pi$ half-plane, in agreement with the behavior at higher Strouhal numbers.

In order to quantify these effects, Fig. 15 plots the relative angle and radial position of the midpoint of each vortex ring. The closed square symbols are for the trailing and combined vortex rings, and the open square symbols are for the leading vortex ring. The incline angle of the leading ring decreases until it is nearly zero and the combined vortex ring eventually exceeds three times the nozzle incline angle. The evolution of the vortex rings shed from the $D/2$, $3D/4$, and D nozzles are also shown. The same general trends occur for each nozzle, and the relative effects are the same as those observed at the larger Strouhal numbers. Namely, the relative increase in incline angle decreases with nozzle incline, and the migration into the $\psi = \pi$ half-plane increases with nozzle incline.

The length of the curve for the leading vortex ring decreases as nozzle incline increases because the pairing occurs closer to the nozzle lip. The pairing for the $D/2$ nozzle occurs around $x/D = 2$. In Fig. 16, the vorticity fields are shown for the $3D/4$ nozzle. In phase $\Phi = 0$, two inclined vortex rings are observed around $x/D = 1.5$, while in phase $\Phi = \pi/2$, the rings have paired. Inclining the vortex rings appears to accelerate the pairing process; however, the nozzle with an incline length of D deviates from these trends somewhat.

In Fig. 17, the velocity and vorticity fields are shown for the D nozzle. Note that, although they are not shown here, the orthogonal data and flow visualization were fundamentally important in determining the complex ring orientation and dynamics. In phase $\Phi = 0$ of the vorticity plots, two in-

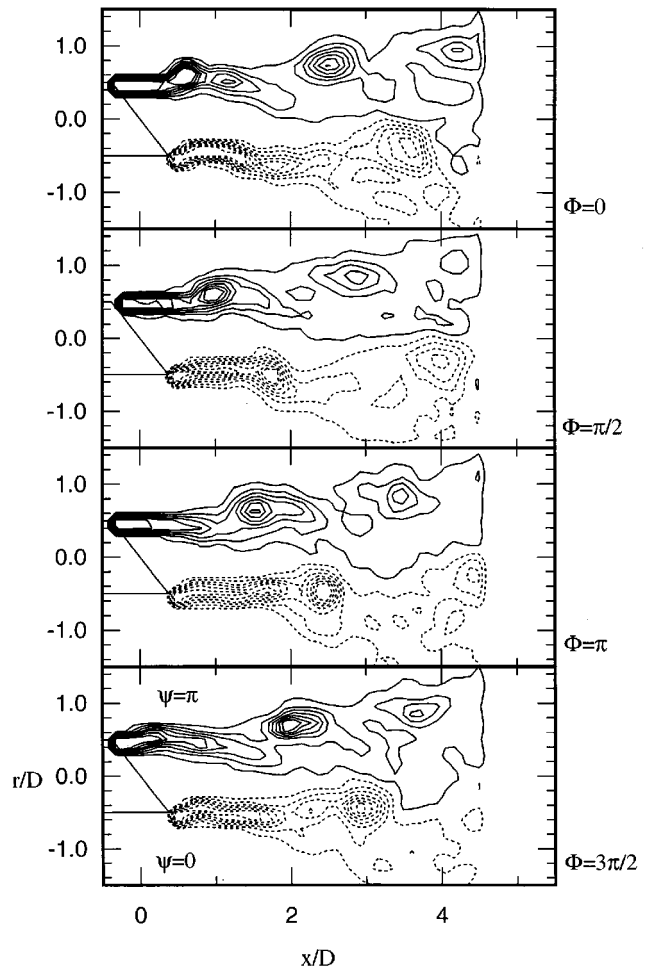


FIG. 16. Ensemble-averaged vorticity field (14 contour levels ranging from $-4U/D$ to $4U/D$) for the $3D/4$ nozzle forced at $St_D = 0.25$ (2.5 Hz) and $u_{\text{rms}}/U = 0.06$. Four phases are shown.

clined vortex rings are observed 1.5 diameters from the nozzle lip. In phase $\Phi = \pi/2$, the vortex core in the $\psi = \pi$ half-plane have combined, while two distinct vortex cores remain in the $\psi = 0$ half-plane centered around $x/D = 2.1$. These cores combine soon afterward, and a single vortex core is observed at $x/D = 2.3$ in the $\Phi = \pi$ plot. Thus, the pairing in the $\psi = \pi$ half-plane occurs even closer to the lip than for the $3D/4$ nozzle (about $1.3D$ from the lip), and the pairing in the $\psi = 0$ half-plane occurs at about $1.8D$ from the nozzle lip. The relative angle and radial location of the vortex ring are shown in Fig. 15. Unlike the cases discussed previously, the trailing and combined vortex ring incline angle do not increase monotonically with downstream distance. When pairing occurs in the $\psi = \pi$ half-plane, the vortex core moves forward slightly and the incline angle is reduced. The subsequent pairing in the $\psi = 0$ half-plane causes an increase in the vortex ring incline angle, and the angle continues to increase downstream. Nozzles with longer incline lengths (up to $2D$) show a similar pairing process when forced at $St_D = 0.25$.

The jet columns shown in Figs. 14(a) and 17(a) have similar characteristics. In particular, the radial spreading rate of the jet is greatly enhanced for the inclined nozzle relative

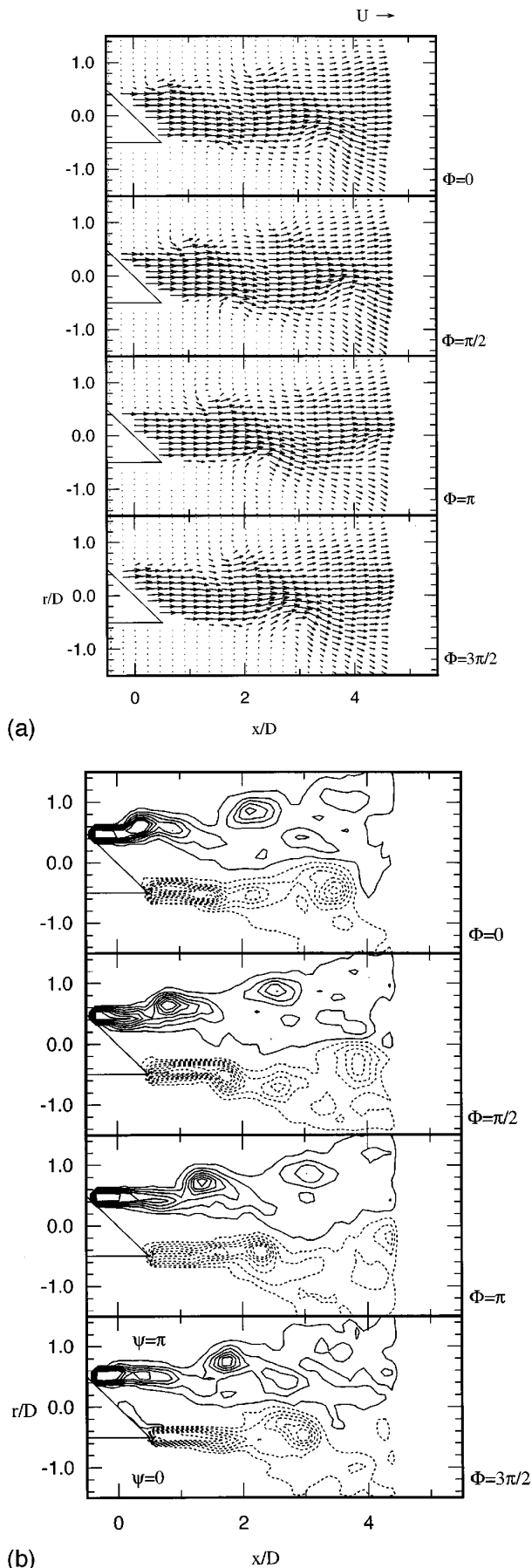


FIG. 17. Ensemble-averaged (a) velocity field, and (b) vorticity field (14 contour levels ranging from $-4U/D$ to $4U/D$) for the D nozzle forced at ($St_D = 0.25$ (2.5 Hz) and $u_{rms}/U = 0.06$). Four phases are shown.

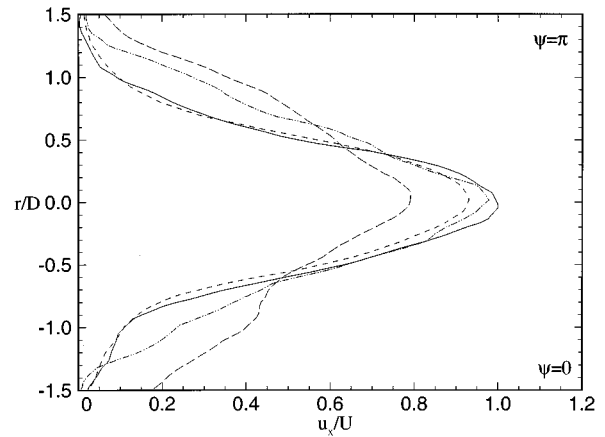


FIG. 18. Axial velocity profiles at $x/D = 4$. — unforced reference nozzle; ---, forced reference nozzle; ····, unforced D nozzle; and - · - ·, forced D nozzle. Forcing at $St_D = 0.25$ (2.5 Hz) and $u_{rms}/U = 0.06$.

to the reference nozzle with the larger increase occurring in the $\psi=0$ half-plane. Figure 18 shows the profiles of axial velocity at $x/D = 4$. The centerline velocity has decreased by about 10% for the forced reference nozzle case relative to the unforced case, but the symmetry of the profile is retained. The unforced flow for the D nozzle showed mild asymmetric radial spreading of the axial velocity. Forcing the flow from the D nozzle caused the centerline velocity to decrease to less than $0.8U$, and the axial velocity to increase significantly for $r/D > 0.5$. This observation is in agreement with previous investigations, which showed that breaking the axisymmetry of the jet enhances mixing and entrainment rates. Forcing at $St_D = 0.5$ and 1.0 yielded the same qualitative trends, although the quantitative effects were smaller.

The second common characteristic of the jet columns in Figs. 14(a) and 17(a) is the serpentine appearance. Close to the D nozzle ($x/D < 2$) the jet column deviates more severely from axisymmetric conditions than the $D/4$ nozzle case. Farther downstream, however, the jet columns appear similar. This is a result of vortex incline angle in the $D/4$ nozzle case increasing much more rapidly than in the D case [see Fig. 15(a)]. The last inclined vortex ring shown in phase $\Phi = \pi/2$ of Fig. 14(b) has an incline angle of 44° , while the same vortex ring has an angle of 48° in the D nozzle case. (The final vortex incline angles observed for the $D/2$ and $3D/4$ nozzles were 43° and 45° , again yielding a similar serpentine jet column.) In Fig. 19, profiles of the axial velocity for each nozzle forced at $St_D = 0.25$ are compared. Each profile shows a reduction of the centerline velocity and a significant increase in axial velocity beyond $r/D = 0.5$. Both effects increase with a nozzle incline angle. Thus, although the jet columns have a similar appearance, the more inclined nozzles are more effective at spreading the axial momentum. Profiles of the radial component of velocity are in complete agreement and reinforce the observation that the radial ejection of fluid is enhanced (particularly in the $\psi=0$ half-plane) by the inclined nozzle.

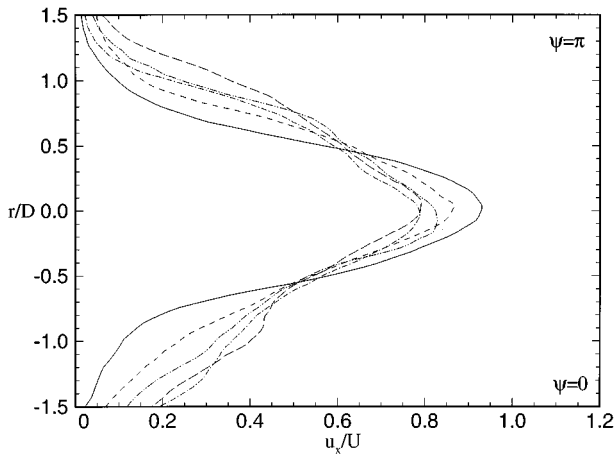


FIG. 19. Axial velocity profiles at $x/D = 4$. — reference; ---, $D/4$; - · - · $D/2$; · · · $3D/4$; and - - - D nozzles. Forcing at $St_D = 0.25$ (2.5 Hz) and $u_{rms}/U = 0.06$.

IV. SUMMARY AND CONCLUSIONS

The round jet flow from nozzles with incline lengths between 0 and D (45°) was examined experimentally. The PIV technique provided quantitative velocity data and the opportunity to track the cores of the vortex rings, while the flow visualization provided qualitative information that greatly assisted our interpretation of the quantitative data. The nozzle incline fundamentally altered the flow field by breaking the axisymmetry of the jet. The radial spreading increased mildly in the unforced flow particularly in the $\psi=0$ half-plane. Forcing amplified the asymmetric radial spreading effects. The radial spreading increased with the nozzle incline angle and decreased with Strouhal number (among those tested). The combination of forcing and nozzle geometry appears to be an effective means of increasing mixing and entrainment in the jet.

The vortex structure consisted of continuous inclined vortex rings for all conditions tested. Vortex rings generally rolled up at angles slightly smaller than the nozzle incline angle. The incline angle of the vortex rings increased with downstream distance, where the greatest relative effect occurred with the least inclined nozzle. The self-induced motion of the inclined vortex rings produced a trajectory into the $\psi=\pi$ half-plane, and the migration from the centerline increased with nozzle incline angle. Forcing at the “preferred” Strouhal number of 0.5 produced inclined vortex rings spaced at a distance D , which showed no inclination to pair. Forcing at larger Strouhal numbers ($St_D = 0.75$ and 1.0) formed inclined vortex rings with smaller spacing. The vortex rings paired around $x/D = 2$ in order to achieve the “preferred” mode. This pairing process was suppressed as the nozzle incline increased because the coherent structure broke down rapidly.

Forcing at $St_D = 0.25$ produced vortex ring pairing for the reference nozzle similar to that observed in previous studies. For the mildly inclined $D/4$ nozzle (14°), the axisymmetric pairing process was altered significantly. The incline angle of the leading vortex ring decreased while it

moved into the $\psi=0$ half-plane. Simultaneously, the trailing vortex moved into the $\psi=\pi$ half-plane and increased its incline angle. The vortex rings eventually paired around $x/D = 2.5$. As the nozzle incline length increased to $3D/4$ (37°) the location of pairing moved closer to the nozzle lip. For the D nozzle, the pairing of the vortex rings occurred approximately $0.5D$ closer to the nozzle lip in the $\psi=\pi$ half-plane than in the $\psi=0$ half-plane. The result was an initial decrease and subsequent increase in vortex incline angle. All other cases showed a monotonic increase.

ACKNOWLEDGMENTS

This work was funded by grants from the McKnight Foundation and the National Science Foundation (CTS-9457014).

- ¹A. Michalke, “On spatially growing disturbances in an inviscid shear layer,” *J. Fluid Mech.* **23**, 521 (1965).
- ²E. Gutmark and C.-M. Ho, “Preferred modes and the spreading rates of jets,” *Phys. Fluids* **26**, 2932 (1983).
- ³S. C. Crow and F. H. Champagne, “Orderly structure in jet turbulence,” *J. Fluid Mech.* **48**, 547 (1971).
- ⁴F. K. Browand and J. Laufer, “The role of large scale structures in the initial development of circular jets,” *Proceedings of the 4th Symposium on the Turbulence in Liquids*, University of Missouri-Rolla, 1975 (Science, Princeton, 1975), pp. 333–334.
- ⁵E. E. Bouchard, Jr. and W. C. Reynolds, “The structure and growth of the mixing layer region of a round jet,” Report No. TF-17, Department of Mechanical Engineering, Stanford University, 1982.
- ⁶A. K. M. F. Hussain and K. B. M. Q. Zaman, “The ‘preferred mode’ of the axisymmetric jet,” *J. Fluid Mech.* **110**, 39 (1981).
- ⁷H. Arbey and J. E. Pflowcs Williams, “Active cancellation of pure tones in an excited jet,” *J. Fluid Mech.* **149**, 445 (1984).
- ⁸R. R. Mankbadi, “The effect of phase-difference on the spreading rate of a jet,” *AIAA J.* **24**, 1941 (1986).
- ⁹T. C. Corke and S. M. Kusek, “Resonance in axisymmetric jets with controlled helical-mode input,” *J. Fluid Mech.* **249**, 307 (1993).
- ¹⁰M. Lee and W. C. Reynolds, “Bifurcating and blooming jets,” Report No. TF-22, Department of Mechanical Engineering, Stanford University, 1985.
- ¹¹D. E. Parekh, A. Leonard, and W. C. Reynolds, “Bifurcating jets at high Reynolds numbers,” Report No. TF-35, Department of Mechanical Engineering, Stanford University, 1988.
- ¹²K. B. M. Q. Zaman, M. F. Reeder, and M. Samimy, “Control of an axisymmetric jet using vortex generators,” *Phys. Fluid* **6**, 778 (1994).
- ¹³S. Zhang and S. P. Schneider, “Quantitative molecular-mixing measurements in a round jet with tabs,” *Phys. Fluids* **7**, 1063 (1995).
- ¹⁴E. Meiburg, J. C. Lasheras, and J. E. Martin, “Experimental and numerical analysis of the three-dimensional evolution of an axisymmetric jet,” *Turbulent Shear Flows 7*, edited by F. Durst, B. E. Launder, F. W. Schmidt, and J. H. Whitelaw (Stanford University, Stanford, 1989).
- ¹⁵F. F. Grinstein, E. Gutmark, and T. Parr, “Near field dynamics of subsonic free square jets. A computational and experimental study,” *Phys. Fluids* **7**, 1483 (1995).
- ¹⁶C.-M. Ho and E. Gutmark, “Vortex induction and mass entrainment in a small-aspect-ratio elliptic jet,” *J. Fluid Mech.* **179**, 383 (1987).
- ¹⁷F. Hussain and H. S. Husain, “Elliptic jets. Part I. Characteristics of unexcited and excited jets,” *J. Fluid Mech.* **208**, 257 (1989).
- ¹⁸R. W. Wlezien and V. Kibens, “Passive control of jets with indeterminate origins,” *AIAA J.* **24**, 1263 (1986).
- ¹⁹V. Kibens and R. W. Wlezien, “Active control of jets from indeterminate-origin nozzles,” *AIAA Paper No. 85-0542*, 1985.
- ²⁰E. K. Longmire and L. H. Duong, “Bifurcating jets generated with stepped and sawtooth nozzles,” *Phys. Fluids* **8**, 978 (1996).
- ²¹E. K. Longmire, J. K. Eaton, and C. J. Elkins, “Control of jet structure by crown-shaped nozzles,” *AIAA J.* **30**, 505 (1992).
- ²²R. W. Wlezien, “Quantitative visualization of acoustically excited jets,” *AIAA Paper No. 88-0499*, 1988.
- ²³V. Kibens, R. W. Wlezien, F. W. Roos, and J. T. Kegelmann, “Trailing-

edge sweep and three-dimensional vortex interactions in jets and mixing layers," AGARD Report No. 438, 1988.

²⁴H. Gründel, "Strukturen in symmetrischen und asymmetrischen Scherschichten," Dissertation, Technische Universität Berlin, Hermann-Föttinger-Institut, 1995.

²⁵D. Liepmann and M. Gharib, "The role of streamwise vorticity in the near-field entrainment of round jets," *J. Fluid Mech.* **245**, 643 (1992).

²⁶J. E. Martin and E. Meiburg, "Numerical investigation of three-dimensionally evolving jets subject to axisymmetric and azimuthal perturbations," *J. Fluid Mech.* **230**, 271 (1991).